Flexible honeycombed nanoporous/glassy hybrid for efficient electrocatalytic hydrogen generation

Rui Li, Xiongjun Liu, Ruoyu Wu, Jing Wang, Zhibin Li, K.C. Chan,* Hui Wang, Yuan Wu, and Zhaoping Lu**

Dr. R. Li, Prof. X. J. Liu, R. Y. Wu, J. Wang, Z. B. Li, Prof. H. Wang, Prof. Y. Wu, Prof. Z. P. Lu
Beijing Advanced Innovation Center for Materials Genome Engineering, State Key Laboratory for Advanced Metals and Materials
University of Science and Technology Beijing
Beijing, 100083, China
E-mail: xjliu@ustb.edu.cn; luzp@ustb.edu.cn

Dr. R. Li, Prof. K. C. Chan
Advanced Manufacturing Technology Research Centre
Department of Industrial and Systems Engineering
The Hong Kong Polytechnic University, Hong Kong
E-mail: kc.chan@polyu.edu.hk

Keywords: nanoporous metals, metallic glasses, hybrid nanostructure, hydrogen evolution reaction (HER), electrocatalysis

Hydrogen evolution reaction (HER) in alkaline media urgently requires electrocatalysts concurrently possessing excellent activity, flexible free-standing capability, and low cost. Herein, a honeycombed nanoporous/glassy sandwich structure fabricated through dealloying metallic glass (MG) is reported. The free-standing hybrid shows outstanding HER performance with a very small overpotential of 37 mV at 10 mA cm^{-2} and a low Tafel slope of 30 mV dec^{-1} in alkaline media, outperforming the commercial Pt/C. By alloying 3 at.% Pt into the MG precursor, a honeycombed $Pt_{75}Ni_{25}$ solid solution nanoporous structure, with fertile active sites and large contact areas for efficient HER, was created on the dealloyed MG surface. Meanwhile, the surface compressive lattice-strain effect was also introduced by substituting the Pt lattice sites with the smaller Ni atoms, which can effectively reduce the hydrogen adsorption energy and thus improve the hydrogen evolution. Moreover, the outstanding stability and flexibility stemming from the ductile MG matrix also make the hybrid suitable for practical electrode application. This work not only offers a reliable strategy

to develop cost-effective and flexible multicomponent catalysts with low Pt usage for efficient HER, but also sheds light on understanding the alloying effects of the catalytic process.

Electrocatalytic water splitting for the sustainable production of hydrogen has been widely regarded as one of the most promising approaches for gaining renewable and clean energy due to its high energy conversion efficiency, simplicity and non-carbon emissions.[1-4] For water electrolysis, the hydrogen evolution reaction (HER) in alkaline electrolyte is deemed to be a more valuable process than acidic HER due to the lack of durable electrocatalysts for oxygen evolution reaction (OER) in acid.[5-7] Although carbon-supported Pt nanoparticles (Pt/C) are the benchmark electrocatalysts with high activity for alkaline HER, the high cost and scarcity essentially limit their widespread commercialization.[8] Consequently, there is considerable interest in discovering cheaper HER catalysts with comparable performance to the commercially available Pt/C in alkaline media. Great efforts have been devoted to enhancing the HER activity of cheap catalysts by alloying, nanostructure modification, and introducing lattice strains on the surfaces,[9-11] and as a result, various nanostructured electrocatalysts with much enhanced HER activity have been developed. However, these nanoscale catalysts are usually pasted on carbon supports mediated by binding materials, which is difficult to industrialize. In this regard, designing self-supported three-dimensional (3D) electrocatalysts is desirable for highly efficient HER.

Recently, free-standing 3D nanoporous materials have attracted close attention owing to their outstanding performance in catalysis.[12-17] The uniform bi-continuous nanoporosity produced by dealloying/etching can offer nanoporous materials satisfactory electrocatalytic activities, high-efficiency electron transportation, and improved selectivity for various redox reactions.[18, 19] To date, numerous nanoporous materials, especially nanoporous transition metals and their oxides, have been reported for efficient catalysts towards HER in alkaline electrolyte.[20-25] However, the brittleness of the dealloyed nanoporous architectures remains

"the Achilles' heel" for their industrialization in flexible/stable electrode devices. More recently, metallic glass (MG) ribbons with good mechanical flexibility have been suggested to be active electrocatalysts for HER due to their metastable state and richness of low-coordination sites at the surface. A few MGs, including Pd-Ni-P, Ni-Fe-P, and Fe-Co-P-C glassy ribbons, have been examined to serve as highly efficient electrocatalysts for water splitting.[26-29] Nevertheless, the HER properties of these MG electrocatalysts are mostly determined in acid, and the low surface area of MG ribbons also limits their electrocatalytic activity.

Therefore, it is highly desirable but challenging to develop novel electrocatalysts to concurrently satisfy all the critical HER requirements in alkaline media, i.e., excellent catalytic activity, flexible free-standing electrode structure, and low Pt usage. Herein, we report a novel flexible self-supported nanoporous/glassy hybrid catalyst for efficient hydrogen evolution. By alloying a small amount of Pt (3 at.%) into a Ni-based MG precursor, a honeycombed $Pt_{75}Ni_{25}$ solid solution nanoporous structure, with fertile active sites and large contact areas, was achieved on the dealloyed MG surface. Meanwhile, the compressive lattice-strain effect was also introduced on the catalyst surface due to the replacement of the Pt lattice sites with the smaller Ni atoms, which can effectively reduce the hydrogen adsorption energy. The synergistic effects of the nanostructure surface and the substitutional solution endow the hybrid electrocatalyst with a very small overpotential of 37 mV at 10 mA cm^{-2} and a low Tafel slope of 30 mV dec^{-1} in alkaline media, outperforming the commercial Pt/C catalyst. Moreover, the outstanding stability and flexibility stemming from the ductile MG matrix make the hybrid suitable for practical applications. The current findings not only provide a novel pathway to develop low cost and flexible HER electrocatalyst with sparing use of Pt, but also are important for further understanding the alloying effects of the catalytic process.

The synthetic route of the nanoporous/glassy hybrids with a sandwich structure is schematically illustrated in **Figure 1**a, which involves the surface dealloying process of the Ni-based MG precursors. In this process, ductile melt-spun $Ni_{40}Zr_{40}Ti_{20-x}Pt_x$ (x=0, 1, 2, 3, 4, and 5 at.%) MG ribbons were used as precursors, the amorphous structures of which were confirmed by X-Ray Diffraction (XRD) (Figure S1, Supporting Information). As an example, Figure 1b shows the dealloyed architecture of the typical $Ni_{40}Zr_{40}Ti_{20}$ MG ribbon etched in 0.025 M HF for 30 min at room temperature. It is clearly seen that a nanoporous surface with bi-continuous pores and ligaments was obtained. Interestingly, a honeycombed structure was created on the surface of the $Ni_{40}Zr_{40}Ti_{17}Pt_3$ MG under the same etching conditions (Figure 1c). Detailed investigation was performed on the relationship between the MG precursor composition and the surface characteristic of the dealloyed products (Figure S2, Supporting Information). As the Pt concentration in the MG precursors increases to 3 at.%, the honeycombed nanostructure starts to form. However, with the further increase of Pt to 5 at.%, the honeycombed structure coarsens gradually. Similar to the ductile precursor ribbons (see Figure 1d), the resultant honeycombed nanoporous/glassy hybrid also exhibits excellent mechanical flexibility, as demonstrated by the manual bending shown in Figure 1e. The fracture surface of the honeycombed nanoporous/glassy hybrid in Figure 1f confirms that the cross-section presents a clear interface between the nanoporous region and the un-dealloyed MG matrix, verifying the hierarchical sandwich structure of the hybrid. The thickness of the nanoporous layers was estimated to be ~285 nm (etched in 0.025 M HF for 30 min). Meanwhile, the vein patterns of the MG matrix also appear along the fracture direction, indicating that the un-dealloyed MG matrix remains amorphous. This observation is consistent with the XRD patterns of the un-dealloyed matrix (Figure S3, Supporting Information).

The HER performance of the nanoporous/glassy hybrids was studied in 1 M KOH aqueous solution using a three-electrode electrochemical system. In this work, the flexible

self-supported hybrid ribbon with a fixed exposing area was directly used as the working electrode (Figure S4, Supporting Information). The electrocatalytic properties of the as-cast, dealloyed $Ni_{40}Zr_{40}Ti_{20-x}Pt_x$ (x=0, 1, 2, 3, 4, and 5 at.%) MG ribbons, and the commercial Pt/C catalyst (20 wt.% Pt) were investigated by linear sweep voltammograms (LSV). The results demonstrate that the un-dealloyed MG ribbon electrodes exhibit weak electrocatalytic effects towards HER (Figure S5, Supporting Information). Under a current density of 10 mA cm^{-2}, the overpotential for the bare nanoporous Ni/glassy hybrid is 97 mV, whilst the overpotential of the honeycombed nanoporous/glassy hybrid by just alloying 3 at.% Pt in the MG precursor significantly decreases to 37 mV (**Figure 2**a and Figure S6 in Supporting Information), much lower than that of the commercial Pt/C electrode (i.e., 51 mV) under the same test conditions. However, the electrocatalytic activity deteriorates as more Pt is added (i.e., >3 at.%). This phenomenon is likely due to the coarsening of the surface honeycombed nanoporous structure (see the surface morphology changes in Figures S2d-f, Supporting Information), which results in a decrease of the electrochemically active surface area (ECSA) and the number of catalytically active sites, as confirmed by the ECSA measurements (Figure S7, Supporting Information). The kinetic behaviors of all the above electrocatalysts during the HER process were further evaluated by the Tafel plots (Figure S8, Supporting Information), which reflects the rate limitation of the electrocatalysis reaction. As shown in Figure 2b, the Tafel slope of the optimal honeycombed nanoporous/glassy hybrid (30 mV dec^{-1}) is lower than that of the Pt/C electrode (31 mV dec^{-1}) and the nanoporous Ni/glassy hybrid (47 mV dec^{-1}), indicating an adequate Volmer-Tafel mechanism in alkaline electrolyte. The HER onset potential of the catalyst electrodes, defined as the potential at a current density of 0.6 mA cm^{-2}, is illustrated in Figure 2c. As can be seen, the honeycombed nanoporous/glassy hybrid also exhibits a lower value of 13 mV, less than that of the Pt/C electrode (19 mV), indicating the high catalytic activity of the honeycombed nanoporous/glassy hybrid. Moreover, the exchange current densities of the aforementioned three catalyst electrodes were evaluated by

extrapolating the Tafel plots (Figure 2c, right axis). As expected, the honeycombed nanoporous/glassy hybrid possesses a maximum value of 0.592 mA cm^{-2}, higher than the bare nanoporous Ni/glassy hybrid (0.088 mA cm^{-2}) and the commercial Pt/C (0.269 mA cm^{-2}), demonstrating its large current at low overpotential and easy activation of HER.

The critical parameters for HER based on our hybrid catalysts were compared with other recently reported HER electrocatalysts in the literature, such as $Pt_3Ni/Ni(OH)_2$,[30] Ni-Mo,[31] NiP/Ni foil,[32] PtCuNi,[33] and other noble metal or transition metal-based nanocatalysts. It is encouraging to see that the performance of the honeycombed nanoporous/glassy hybrid catalyst, such as low overpotential and Tafel slope, is superior to most previously reported catalysts in alkaline solution (Figure 2d and Table S1, Supporting Information). The electrode reaction kinetics of the honeycombed nanoporous/glassy hybrid is more evident in electrochemical impedance spectra (EIS). The Nyquist plots reveal a low charge transfer resistance of the dealloyed honeycombed nanoporous/glassy hybrid, implying that the most efficient HER kinetics is achieved at the hybrid/electrolyte interface (Figure 2e). The dependence of the charge transfer resistance on the Pt content in the MG precursors (Figure S9, Supporting Information) is related to the synergistic effects of the nanoporous structure and the catalytically active sites. By alloying Pt into the MG precursor, the bi-continuous honeycombed nanoporous structure forms and the number of catalytically active sites on the surface increases, leading to lower charge-transfer resistance of HER. However, when the alloying Pt content exceeds an appropriate value (i.e., 3 at.%), the nanoporosity starts to coarsen (Figures S2d-f, Supporting Information), which significantly reduces the ECSA (Figure S7h, Supporting Information) and hinders the efficient contact between the catalyst and the electrolyte, thus leading to the rebound of the charge transfer resistance. In addition to the electrocatalytic activity, stability is also an important factor for HER application. The long-term durability of the honeycombed nanoporous/glassy hybrid was investigated by continuous cyclic voltammetry (CV) tests, and as illustrated in Figure 2f, the hybrid electrode

shows cycling retention with less than a 2 mV overpotential increase at 10 mV cm^{-2} after 1000 CV cycles. Long-term HER testing at a current density of 10 mV cm^{-2} (the inset in Figure 2f) vividly confirms the outstanding stability of the honeycombed electrode over a period of 72 h. Moreover, the Faradaic efficiency of the hybrid catalyst was determined by gas chromatography measurement (Figure S10, Supporting Information), the detected H_2 amount is well fitted with the theoretical calculation for a nearly 100% Faradaic efficiency, further demonstrating the high efficiency and durability. Based on all these results, our honeycombed nanoporous/glassy hybrid exhibits excellent HER electrochemical activity and kinetic property, that is, a lower overpotential value, a higher exchange current density, a much lower Tafel slope, excellent stability, and nearly 100% Faradaic efficiency for HER in alkaline electrolyte, as compared with the commercial Pt/C electrode. More importantly, the turnover frequency (TOF) versus overpotential plots (Figure S11, Supporting Information) were obtained based on the measured ECSA and the estimated numbers of active sites. Remarkably, the TOF value of the honeycombed nanoporous/glassy hybrid is up to 0.89 H_2 s^{-1} at 100 mV in 1 M KOH, 19.3 and 1.8 times higher than the nanoporous Ni/glassy hybrid (0.046 H_2 s^{-1}) and the 20 wt.% commercial Pt/C (0.49 H_2 s^{-1}), respectively, clearly demonstrating the superior intrinsic electrocatalytic activity.

As mentioned above, the sandwich hybrid with a honeycombed nanoporous surface fabricated using the MG precursor containing only 3 at.% Pt shows outstanding HER performance, and then two critical questions are naturally raised: how do these unique nanostructures form during dealloying and why can such hybrid structure offer outstanding HER activity (even better than the commercial Pt/C)? To explain these mysteries, detailed microstructure characterizations of the honeycombed nanoporous structure were conducted. Typically, **Figure 3**a shows the transmission electron microscopy (TEM) image of the surface that resulted from the dealloying of the $Ni_{40}Zr_{40}Ti_{17}Pt_3$ MG, where edges with a width of ~20 nm of the honeycombed structure are clearly observed. The scanning transmission electron

microscopy (STEM) elemental mapping shown in Figure 3b reveals that the edges are enriched with Pt, although the MG precursor only contains 3 at.% Pt. The TEM-EDS analysis indicates that the atomic ratio of Pt to Ni in the Pt-rich edges is close to 3:1 (Figure S12, Supporting Information). The obvious Pt aggregation on the honeycombed surface structure is due to the phase segregation of Pt from Ni during dealloying. A similar phenomenon was also observed in the formation of nanocrystalline Pt_3Ni and Pt_3Co by other corrosion methods.[30, 34, 35] The surface states of the Pt-rich honeycombed surface structure were also investigated by XPS (Figure 3c). The Ni 2p XPS spectrum consists of metallic Ni^0 and two more peaks attributed to Ni^{2+}, indicating that the hybrid surface contains metallic Ni as well as unavoidable oxides.[36] The Pt 4f spectrum consists of two peaks for metallic Pt with binding energy of 71.21 (Pt $4f_{7/2}$) and 74.56 eV (Pt $4f_{5/2}$), respectively. The value of the energy separation of 3.35 eV is in good agreement with that reported in the literature. [37, 38] Note that the binding energy of Pt^0 is larger than the reported value of 71.1 eV for pure Pt. This discrepancy could be attributed to the electronic hybridization and the alloying effect of Ni into Pt. Besides, the XPS analysis also shows that the surface composition of the hybrid is close to $Pt_{75}Ni_{25}$, in good agreement with the EDS result and the inductively coupled plasma-optical emission spectrometer (ICP-OES) measurements (Table S2, Supporting Information). The grazing-incidence XRD result confirms that the honeycombed $Pt_{75}Ni_{25}$ nanoporous layer has a face-centered cubic (fcc) solid solution structure (Figure S13, Supporting Information). Nevertheless, it is noted that all the peak positions are shifted towards higher angles than those of the perfect fcc Pt, identifying the lattice contraction in the $Pt_{75}Ni_{25}$ solid solution due to the substitution of Pt by the smaller Ni. This result also suggests the presence of a compressive lattice-strain effect in the dealloyed honeycombed $Pt_{75}Ni_{25}$ structure. Furthermore, the interconnected nanoporous structure below the Pt-rich honeycombed surface was also characterized by TEM (Figure 3d). The HRTEM image shows a 3D morphology of the porous structure with concave and convex curvatures, and the average ligament size is

estimated to be ~6 nm (Figure 3e). STEM elemental mapping and EDS analysis of the selected nanoporous structure and the magnified ligaments (Figures S14, 15, Supporting Information) indicate that Pt and Ni elements are uniformly distributed throughout the bottom nanoporous channels and the atomic ratio of Pt and Ni is about 1:1. Meanwhile, the characterization of the interface between the nanoporous structure and the MG substrate shows that the dealloyed (Ni, Pt) solid solutions, i.e., the ligaments, grow epitaxially from the MG surface (Figure 3f). The corresponding SAED patterns further prove the polycrystalline nature of the dealloyed (Pt, Ni) ligaments in the bottom (upper right in Figure 3f) and the amorphous state of the residual MG matrix (lower right in Figure 3f). According to the diffraction rings, the calculated lattice parameter of the dealloyed (Pt, Ni) ligaments is approximately 0.3801 nm, smaller than that of the pure fcc Pt (0.3924 nm). This observation further demonstrates the shrinking effect resulting from the substitution of the Pt lattice sites with Ni atoms, which would enhance the HER activity of the hybrid surface.

To reveal the formation mechanism of the honeycombed Pt-rich nanostructure, we systemically investigated the evolution of the surface morphology of the specially designed $Ni_{40}Zr_{40}Ti_{17}Pt_3$ MG precursor during dealloying (Figure S16, Supporting Information). It is noted that the diversity in the standard electrode potential between Ni and Zr/Al results in different dissolution rates during dealloying. As illustrated in Figure 3g, the easy dissolution of Zr/Al elements and the surface diffusion of Ni/Pt elements give rise to the formation of the (Pt, Ni) ligaments of the initial hollow structure. Upon further dealloying, the residual Ni is also partially removed from the hollow structure. Due to the particular elemental segregation which usually occurs in the Ni-Pt system,[39, 40] the Pt-rich phases tend to anisotropically grow along the specific crystallographic orientations of (111) and (200). As the growth time is prolonged, the Pt-rich phases selectively migrate outwards to the surface, eventually leading to the formation of the honeycomb-shaped nanostructure with $Pt_{75}Ni_{25}$ solid solutions. Apparently, the Pt-rich honeycombed nanoporous structure is mainly responsible for the

superior HER performance. First, the combination of the dealloyed bi-continuous nanoporosity and the honeycombed $Pt_{75}Ni_{25}$ solid solution structure can provide a large specific surface area (Figure S17, Supporting Information) and ECSA (Figure S7, Supporting Information), attributing to the exposure of rich catalytically active sites for fast electrochemical reaction kinetics. Second, the honeycombed $Pt_{75}Ni_{25}$ solid solution nanoporous structure can further facilitate electrolyte penetration and ion diffusion, giving rise to the low charge transfer resistance (Figure S9, Supporting Information) for efficient HER kinetics. Third, as evidenced by the TOF results (Figure S11, Supporting Information), which is the intrinsic reason for HER activity, the honeycombed $Pt_{75}Ni_{25}$ solid solution structure can promote water dissociation with high TOF, making it conducive for H_2 generation and release. Moreover, the open and hollow nano-frame structure of the honeycombed $Pt_{75}Ni_{25}$ solid solution exhibits good stability (Figures S18, 19 and Table S3, Supporting Information), which can effectively accommodate the volume expansion of the active sites in the electron transportation process and enable easy release of the evolved H_2 gas bubbles during the long-term HER, thus avoiding the dramatic decline of the hydrogen evolution activity and leading to the excellent electrocatalytic durability.

In addition to the honeycombed nanoporous structure, the alloying effect of Ni in Pt is also essentially beneficial for the superior HER activity of the hybrid. To further clarify this point, density functional theory (DFT) calculations were carried out. The Gibbs free energy of hydrogen adsorption (ΔG_{H^*}) is a critical parameter to predict theoretical activity for HER, and the absolute value of ΔG_{H^*} is close to thermoneutral (i.e., $\Delta G_{H^*} \approx 0$) for a desirable electrocatalyst. [41, 42] In what follows, ΔG_{H^*} of the three models, $Pt_{75}Ni_{25}$, pure Ni, and pure Pt, was calculated. For the $Pt_{75}Ni_{25}$ (111) surface, different H adsorption sites including Pt (top), Ni (top), Pt-Pt-Ni (fcc), and Pt-Pt-Pt (hcp) were systematically investigated (**Figure 4**a and Figure S20 in Supporting Information). For the comparative Ni (111) and Pt (111) surfaces,

we studied three possible adsorption sites, i.e., the top, fcc, and hcp sites. The corresponding structure models are shown in Figures S21, 22 (Supporting Information), respectively. According to the calculated results of the different models (Figure 4b and Tables S4-6, Supporting Information), the Pt (top) site on the $Pt_{75}Ni_{25}$ (111) surface exhibits the smallest $|\Delta G_{H^*}|$ value of 0.127 eV among the modelled $Pt_{75}Ni_{25}$ (111) surfaces, which is also lower than that of the optimal Ni (111) hcp site (0.223 eV) and Pt (111) top site (0.185 eV). Therefore, from a thermodynamic point of view, the $Pt_{75}Ni_{25}$ surface possesses superior HER activity than pure Ni or Pt. These results demonstrate that by alloying smaller atoms like Ni into Pt, the surface compressive lattice strain which can affect the electronic charge redistribution of the catalyst surface can be introduced on the hybrid surface.[10, 43, 44] Thus, the surface energy of Pt can be decreased and the hydrogen adsorption becomes easier, eventually resulting in an improved hydrogen evolution activity of the hybrid. Moreover, the water molecule adsorption energies for different models were calculated as well. As shown in Figure 4c, the hybrid surface with Pt and Ni shows a more negative water adsorption energy (ΔE_{H_2O} =-0.933 eV) than that of pure Ni (ΔE_{H_2O} =-0.807 eV) and Pt (ΔE_{H_2O} =-0.801 eV), implying a more favorable formation of the catalyst-H_2O (initial state) on the surface of the honeycombed nanostructure. This observation further confirms that the alloying addition of Ni is beneficial in enhancing HER activity. All these calculated results, together with the experimental data, manifest that the outstanding HER activity of the hybrid originates from the synergistic effects of the honeycombed $Pt_{75}Ni_{25}$ nanoporous structure and the substitutional solid solution of the smaller Ni atoms into the Pt lattices. It is important to point out that with our current synthesis method, massive Pt-rich active spots can be achieved with low Pt usage in the MG precursor.

Additionally, the relationship between HER activity, flexibility, and nanoporous layer thickness of the honeycombed nanoporous/glassy hybrid were investigated. Honeycombed

nanoporous/glassy hybrids with different thicknesses of the nanoporous layers from 48 to 2137 nm were fabricated by using HF solutions with different concentrations. Bending experiments were adopted to determine the flexural toughness of the hybrids and the HER performances of these hybrids were also tested. As shown in **Figure 5**, the hybrids tend to be brittle with the increase of the nanoporous layer thickness. In particular, the hybrids are flexible as long as the nanoporous layer thickness is below 1271 nm (bending degree: 180°). From the standpoint of the HER activity, nevertheless, the nanoporous layer thickness has a preferable range from 197 to 442 nm due to the formation of the honeycombed Pt-rich nanoporous surface structure during dealloying. When the thickness exceeds 442 nm, the overpotential increases because of the weakening of the surface compressive lattice strain resulting from the over-dissolution of Ni from the Pt-rich honeycombed structure. As a result, the optimum nanoporous layer thickness for the hybrid to simultaneously achieve excellent HER activity, good flexibility, and structure stability falls in the range of 197 to 442 nm. This finding indicates that by the controlling dealloying conditions, the resultant honeycombed nanoporous/glassy hybrid can be directly used as an electrode device without using any binders and additives in practice and exhibits superior electrochemical stability to other conventional discrete particulate HER catalysts.

In summary, we have developed novel flexible free-standing nanoporous/glassy hybrids with tunable nanostructures and catalytic activities by surface dealloying of Ni-based MG precursors. Particularly, a Pt-rich honeycombed structure can be obtained by alloying a small amount of Pt into the MG precursor. The resultant flexible honeycombed nanoporous/glassy hybrid can be directly used as electrocatalyst electrode, and exhibits excellent HER performance with a low overpotential of 37 mV at 10 mA cm^{-2} and a small Tafel slope of 30 mV dec^{-1} in alkaline solution, superior to the commercial Pt/C catalyst (20 wt.% Pt). Combined with the theoretical calculations, the outstanding activity of the hybrid catalyst for HER can be attributed to the synergistic effects of the dealloyed $Pt_{75}Ni_{25}$ honeycombed

nanoporous structure which not only increases the number of active sites and contact areas but also induces the surface compressive lattice-strain effect resulting from the substitution of smaller Ni atoms in the Pt lattices. Our finding not only provides an easy and effective way to develop flexible, cost-effective multicomponent catalysts for efficient HER in alkaline media with sparing use of Pt, but also sheds light on understanding the alloying effects of the catalytic process.

Supporting Information
Supporting Information is available from the Wiley Online Library or from the author.

Acknowledgements
This research was supported by National Natural Science Foundation of China (Nos. 51671018, 51671021, 11790293, 51871016, and 51531001), 111 Project (B07003), Program for Changjiang Scholars and Innovative Research Team in University of China (IRT_14R05) and the Projects of SKLAMM-USTB (2018Z-01, 2018Z-19). This research was also supported by the Hong Kong Polytechnic University Postdoctoral Fellowships Scheme (1-YW3D).

Conflict of Interest
The authors declare no conflict of interest.

Received: ((will be filled in by the editorial staff))
Revised: ((will be filled in by the editorial staff))
Published online: ((will be filled in by the editorial staff))

References

[1] S. Chu, A. Majumdar, *Nature* **2012**, *488*, 294.

[2] T. Wang, H. Xie, M. Chen, A. D'Aloia, J. Cho, G. Wu, Q. Li, Nano Energy **2017**, *42*, 69.

[3] A. Eftekhari, *Int. J. Hydrogen Energ.* **2017**, *42*, 11053.

[4] F. Yu, H. Zhou, Z. Zhu, J. Sun, R. He, J. Bao, S. Chen, Z. Ren, *ACS Catal.* **2017**, *7*, 2052.

[5] J. Lai, B. Huang, Y. Chao, X. Chen, S. Guo, *Adv. Mater.* **2019**, *31*, 1805541.

[6] J. Su, Y. Yang, G. Xia, J. Chen, P. Jiang, Q. Chen, *Nat. Commun.* **2017**, *8*, 14969.

[7] L. C. Seitz, C. F. Dickens, K. Nishio, Y. Hikita, J. Montoya, A. Doyle, C. Kirk, A. Vojvodic, H. Y. Hwang, J. K. Norskov, *Science* **2016**, *353*, 1011.

[8] J. Yu, Y. Guo, S. She, S. Miao, M. Ni, W. Zhou, M. Liu, Z. Shao, *Adv. Mater.* **2018**, *30*, 1800047.

[9] S. Y. Tee, K. Y. Win, W. S. Teo, L. D. Koh, S. Liu, C. P. Teng, M. Y. Han, *Adv. Sci.* **2017**, *4*, 1600337.

[10] M. Shao, J. H. Odell, A. Peles, D. Su, *Chem. Commun.* **2014**, *50*, 2173.

[11] O. Aaboubi, A. Y. Ali-Omar, E. Dzoyem, J. Marthe, M. Boudifa, *J. Power Sources* **2014**, *269*, 597.

[12] J. Zhang, C. M. Li, *Chem. Soc. Rev.* **2012**, *41*, 7016.

[13] A. Welch, J. S. DuChene, G. Tagliabue, A. R. Davoyan, W. Cheng, H. A. Atwater, *ACS Appl. Energy Mater.* **2019**, *2*, 164.

[14] Z. Tu, M. J. Zachman, S. Choudhury, S. Wei, L. Ma, Y. Yang, L. F. Kourkoutis, L. A. Archer, *Adv. Energy Mater.* **2017**, *7*, 1602367.

[15] Y. Ito, W. Cong, T. Fujita, Z. Tang, M. Chen, *Angew. Chem.* **2015**, *127*, 2159.

[16] C. Yang, M. Gao, Q. Zhang, J. Zeng, X. Li, A. Abbott, *Nano Energy* **2017**, *36*, 85.

[17] R. Yao, Y. Zhou, H. Shi, Q. Zhang, L. Gu, Z. Wen, X. Lang, Q. Jiang, *ACS Energy Lett.* **2019**, *4*, 1379.

[18] X. Lang, A. Hirata, T. Fujita, M. Chen, *Nat. Nanotechnol.* **2011**, *6*, 232.

[19] T. Fujita, P. Guan, K. McKenna, X. Lang, A. Hirata, L. Zhang, T. Tokunaga, S. Arai, Y. Yamamoto, N. Tanaka, *Nat. Mater.* **2012**, *11*, 775.

[20] C. Dong, T. Kou, H. Gao, Z. Peng, Z. Zhang, *Adv. Energy Mater.* **2018**, *8*, 1701347.

[21] M. Gong, D. Y. Wang, C. C. Chen, B. J. Hwang, H. Dai, *Nano Res.* **2016**, *9*, 28.

[22] F. Safizadeh, E. Ghali, G. Houlachi, *Inter. J. Hydrogen Energ.* **2015**, *40*, 256.

[23] Z. Cao, Q. Chen, J. Zhang, H. Li, Y. Jiang, S. Shen, G. Fu, B.-a. Lu, Z. Xie, L. Zheng, *Nat. Commun.* **2017**, *8*, 15131.

[24] Y. Ji, L. Yang, X. Ren, G. Cui, X. Xiong, X. Sun, *ACS Sustain. Chem. Eng.* **2018**, *6*, 11186.

[25] J. Sun, Z. Wen, L. Han, Z. Chen, X. Lang, Q. Jiang, *Adv. Funct. Mater.* **2018**, *28*, 1706127.

[26] Y. Hu, Y. Wang, R. Su, C. Cao, F. Li, C. Sun, Y. Yang, P. Guan, D. Ding, Z. Wang, *Adv. Mater.* **2016**, *28*, 10293.

[27] Y. Tan, F. Zhu, H. Wang, Y. Tian, A. Hirata, T. Fujita, M. Chen, *Adv. Mater. Interfaces* **2017**, *4*, 1601086.

[28] F. Hu, S. Zhu, S. Chen, Y. Li, L. Ma, T. Wu, Y. Zhang, C. Wang, C. Liu, X. Yang, *Adv. Mater.* **2017**, *29*, 1606570.

[29] F. Zhang, J. Wu, W. Jiang, Q. Hu, B. Zhang, *ACS Appl. Mater. Inter.* **2017**, *9*, 31340.

[30] C. Chen, Y. Kang, Z. Huo, Z. Zhu, W. Huang, H. L. Xin, J. D. Snyder, D. Li, J. A. Herron, M. Mavrikakis, *Science* **2014**, *343*, 1339.

[31] J. Zhang, T. Wang, P. Liu, S. Liu, R. Dong, X. Zhuang, M. Chen, X. Feng, *Energ. Environ. Sci.* **2016**, *9*, 2789.

[32] M. Ledendecker, S. Krick Calderón, C. Papp, H. P. Steinrück, M. Antonietti, M. Shalom, *Angew. Chem. Int. Edit.* **2015**, *54*, 12361.

[33] Y. Shen, A. C. Lua, J. Xi, X. Qiu, *ACS Appl. Mater. Inter.* **2016**, *8*, 3464.

[34] N. Becknell, Y. Kang, C. Chen, J. Resasco, N. Kornienko, J. Guo, N. M. Markovic, G. A. Somorjai, V. R. Stamenkovic, P. Yang, *J. Am. Chem. Soc.* **2015**, *137*, 15817.

[35] N. Becknell, C. Zheng, C. Chen, Y. Yu, P. Yang, *Surf. Sci.* **2016**, *648*, 328.

[36] H. Qiu, Y. Ito, W. Cong, Y. Tan, P. Liu, A. Hirata, T. Fujita, Z. Tang, M. Chen, *Angew. Chem. Int. Edit.* **2015**, *54*, 14031.

[37] Y. Wang, K. Yin, L. Lv, T. Kou, C. Zhang, J. Zhang, H. Gao, Z. Zhang, *J. Mater. Chem. A* **2017**, *5*, 23651.

[38] S. Fu, C. Zhu, J. Song, M. H. Engelhard, Y. He, D. Du, C. Wang, Y. Lin, *J. Mater.*

Chem. A **2016**, *4*, 8755.

[39] Z. Niu, N. Becknell, Y. Yu, D. Kim, C. Chen, N. Kornienko, G. A. Somorjai, P. Yang, *Nat. Mater.* **2016**, *15*, 1188.

[40] N. Zhang, Q. Shao, X. Xiao, X. Huang, *Adv. Funct. Mater.* **2019**, *29*, 1808161.

[41] X. Kong, K. Xu, C. Zhang, J. Dai, S. Norooz Oliaee, L. Li, X. Zeng, C. Wu, Z. Peng, *ACS Catal.* **2016**, *6*, 1487.

[42] C. Zhu, A. L. Wang, W. Xiao, D. Chao, X. Zhang, N. H. Tiep, S. Chen, J. Kang, X. Wang, J. Ding, *Adv. Mater.* **2018**, *30*, 1705516.

[43] K. Tedsree, T. Li, S. Jones, C. W. A. Chan, K. M. K. Yu, P. A. Bagot, E. A. Marquis, G. D. Smith, S. C. E. Tsang, *Nat. Nanotechnol.* **2011**, *6*, 302.

[44] J. R. Kitchin, J. K. Nørskov, M. A. Barteau, J. Chen, *Phys. Rev. Lett.* **2004**, *93*, 156801.

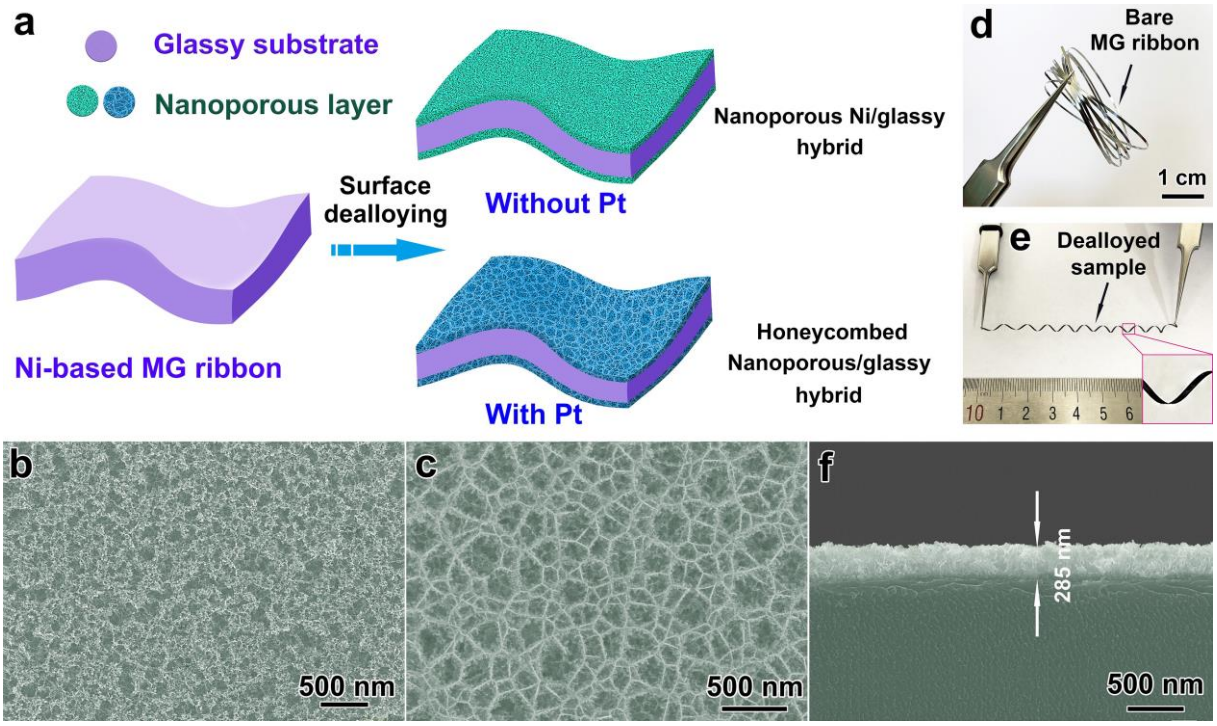

Figure 1. Fabrication and morphologies of the nanoporous/glassy hybrids. a) Schematic illustration of the fabrication process of the nanoporous/glassy hybrids. b) Surface morphology of the dealloyed $Ni_{40}Zr_{40}Ti_{20}$ MG ribbon. c) Surface morphology of the dealloyed $Ni_{40}Zr_{40}Ti_{17}Pt_3$ MG ribbon. d) Optical photograph of the as-cast MG ribbon. e) Optical photograph of the surface dealloyed MG ribbon and its flexibility. The inset shows the color change of the dealloyed sample. f) SEM cross-sectional image of the produced honeycombed nanoporous/glassy hybrid.

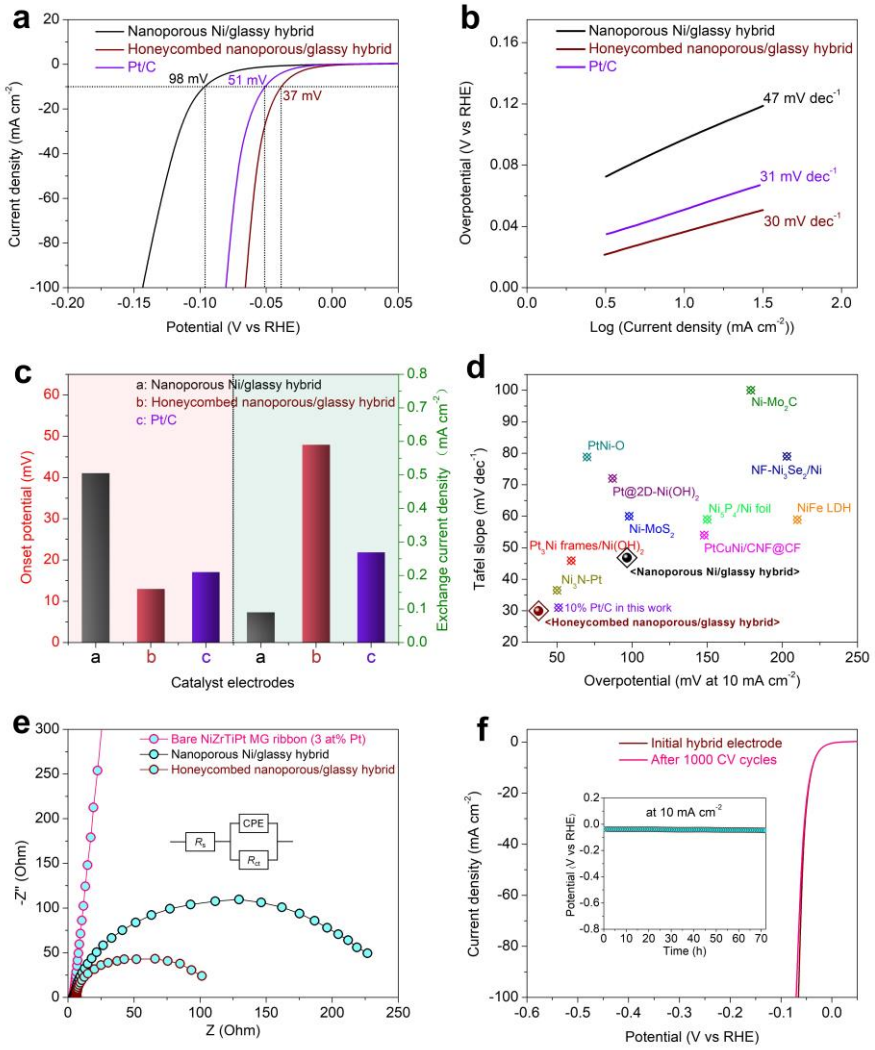

Figure 2. HER electrocatalytic activities of the hybrid catalysts. a) Polarization curves of the surface dealloyed $Ni_{40}Zr_{40}Ti_{20-x}Pt_x$ MG (x=0, 1, 2, 3, 4, and 5 at.%) and Pt/C catalyst electrodes in 1 M KOH aqueous electrolyte. b) Tafel slopes of the nanoporous Ni/glassy hybrid, honeycombed nanoporous/glassy hybrid, and Pt/C electrocatalyst from the polarization curves. c) Onset potentials (left axis) and exchange current densities (right axis) of the nanoporous Ni/glassy hybrid, honeycombed nanoporous/glassy hybrid, and Pt/C electrocatalyst. d) Comparison of the HER activities with some recently reported HER electrocatalysts in alkaline solutions. e) Nyquist plots of the bare $Ni_{40}Zr_{40}Ti_{17}Pt_3$ MG, nanoporous Ni/glassy hybrid, and honeycombed nanoporous/glassy hybrid. f) Polarization curves of the honeycombed nanoporous/glassy hybrid electrode before and after 1000 CV cycles. The inset is the long-term HER stability test of the electrocatalyst at the current density of 10 mA cm^{-2}.

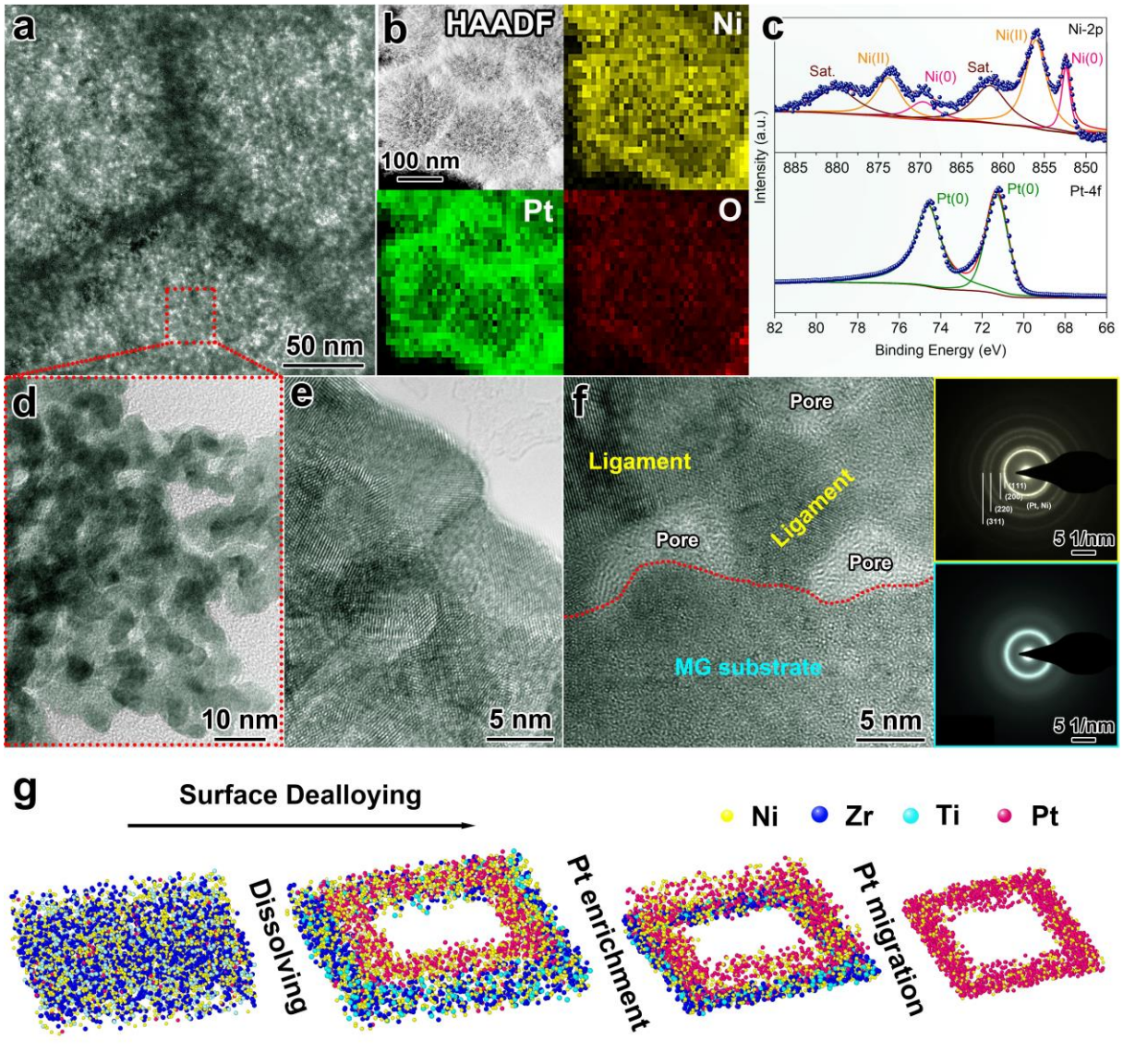

Figure 3. Structural characterizations and formation mechanism of the honeycombed nanoporous/glassy hybrid. a) TEM image of the honeycombed nanoporous structure of the dealloyed $Ni_{40}Zr_{40}Ti_{17}Pt_3$ MG. b) HAADF-STEM image and its corresponding elemental mapping of the honeycombed surface structure. c) XPS spectra of Ni 2p and Pt 4f for the surface honeycombed surface structure. d) TEM image of the bottom nanoporous structure. e) HRTEM of the interconnected nanoporous structure. f) HRTEM of the interface between the (Pt, Ni) ligaments and the un-dealloyed MG matrix. SAED patterns of the dealloyed (Pt, Ni) ligaments (upper right) and the MG matrix (lower right). g) Schematic illustration of the formation of the honeycombed $Pt_{75}Ni_{25}$ surface structure during the dealloying process.

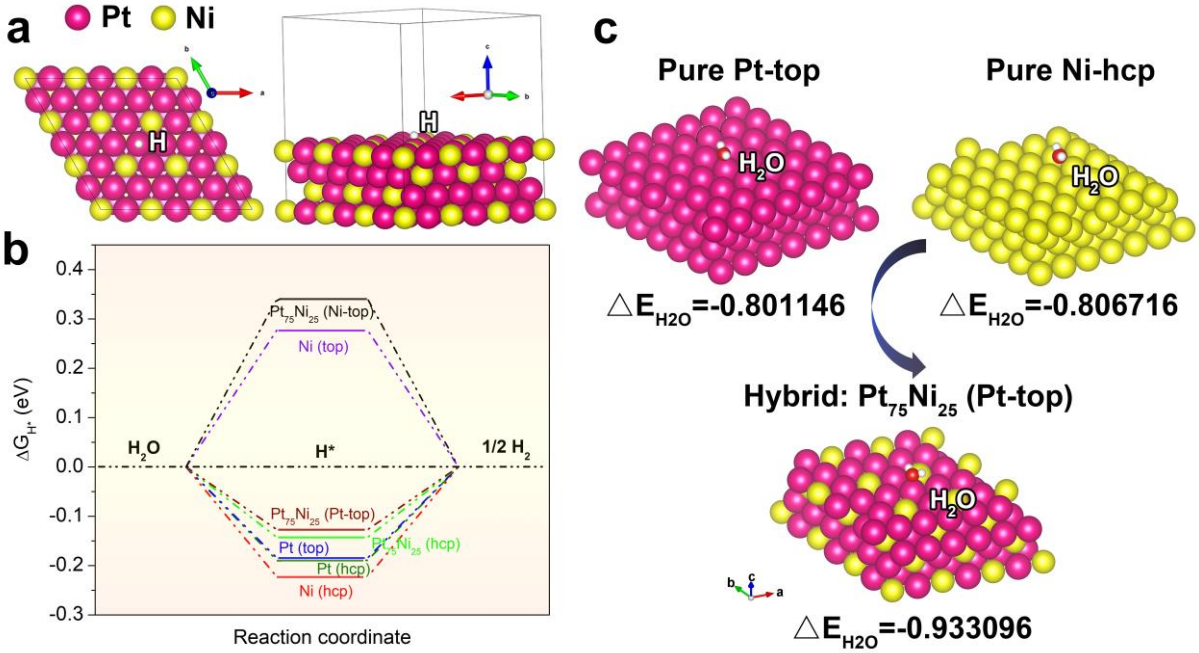

Figure 4. Theoretical calculations. a) Atomic configuration of the $Pt_{75}Ni_{25}$ (Pt-top) model and the adsorption site of H*. b) Calculated free-energy changes in different models. c) Water adsorption energies for the Ni hcp, Pt top, and $Pt_{75}Ni_{25}$ (Pt-top) models.

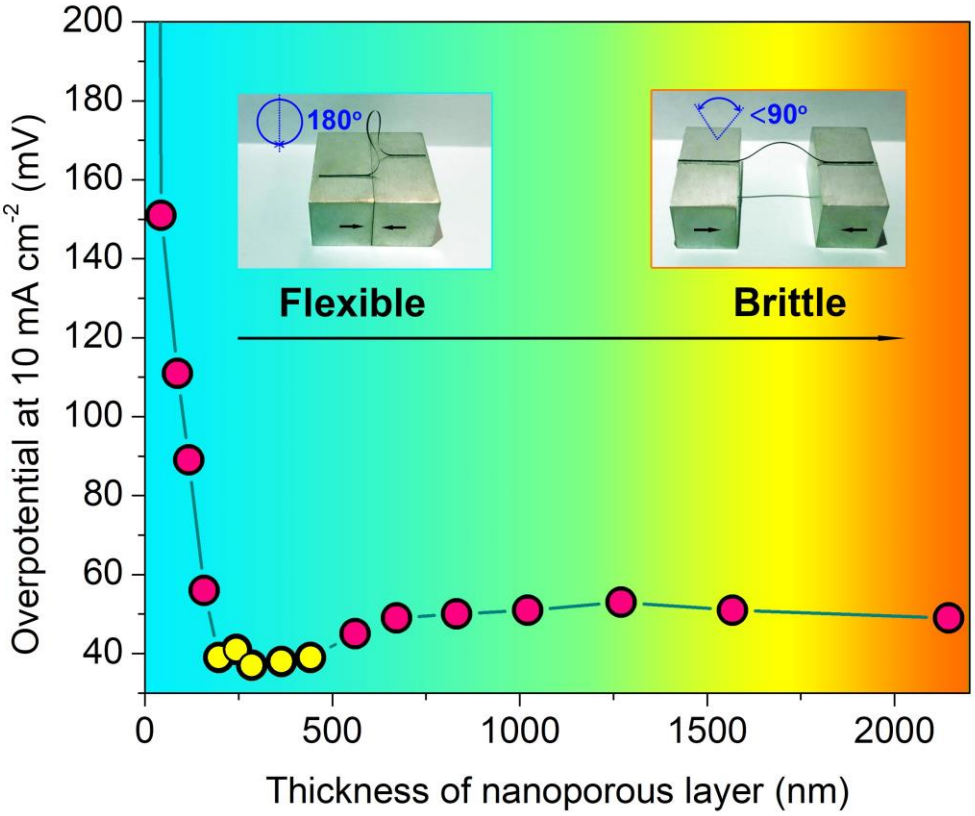

Figure 5. Dependence of HER activity and flexibility on the nanoporous layer thickness of the honeycombed nanoporous/glassy hybrid. Insets show the bending experiments of the hybrids with the nanoporous layer thicknesses of ~285 nm (left) and ~1568 nm (right), respectively.